A joint atmosphere-ocean inversion for surface fluxes of carbon dioxide: 1. Methods and global-scale fluxes

Andrew R. Jacobson,[1,2] Sara E. Mikaloff Fletcher,[1,3] Nicolas Gruber,[3,4] Jorge L. Sarmiento,[1] and Manuel Gloor[1,5]

Received 27 May 2005; revised 4 November 2006; accepted 20 November 2006; published 17 March 2007.

[1] We have constructed an inverse estimate of surface fluxes of carbon dioxide using both atmospheric and oceanic observational constraints. This global estimate is spatially resolved into 11 land regions and 11 ocean regions, and is calculated as a temporal mean for the period 1992–1996. The method interprets in situ observations of carbon dioxide concentration in the ocean and atmosphere with transport estimates from global circulation models. Uncertainty in the modeled circulation is explicitly considered in this inversion by using a suite of 16 atmospheric and 10 oceanic transport simulations. The inversion analysis, coupled with estimates of river carbon delivery, indicates that the open ocean had a net carbon uptake from the atmosphere during the period 1992–96 of 1.7 PgC yr^{-1}, consisting of an uptake of 2.1 PgC yr^{-1} of anthropogenic carbon and a natural outgassing of about 0.5 PgC yr^{-1} of carbon fixed on land and transported through rivers to the open ocean. The formal uncertainty on this oceanic uptake, despite a comprehensive effort to quantify sources of error due to modeling biases, uncertain riverine carbon load, and biogeochemical assumptions, is driven down to 0.2 PgC yr^{-1} by the large number and relatively even spatial distribution of oceanic observations used. Other sources of error, for which quantifiable estimates are not currently available, such as unresolved transport and large region inversion bias, may increase this uncertainty.

Citation: Jacobson, A. R., S. E. Mikaloff Fletcher, N. Gruber, J. L. Sarmiento, and M. Gloor (2007), A joint atmosphere-ocean inversion for surface fluxes of carbon dioxide: 1. Methods and global-scale fluxes, *Global Biogeochem. Cycles*, *21*, GB1019, doi:10.1029/2005GB002556.

1. Introduction

[2] Since the mid-1950s, when consistent records of atmospheric carbon dioxide measurements at widely separated stations first became available, researchers have recognized the existence of persistent spatial concentration gradients and attempted to make inferences from them on how the carbon cycle operates [*Keeling*, 1960]. That these gradients endure in the face of constant mixing by atmospheric circulation implies the existence of persistent surface sources and sinks of CO_2. Extensive work has been done to localize and quantify these fluxes of carbon, generally by estimating surface fluxes for a discrete set of land and ocean regions in the context of atmospheric transport inversions [e.g., *Bolin and Keeling*, 1963; *Keeling et al.*, 1989; *Enting and Mansbridge*, 1989; *Tans et al.*, 1989; *Fan et al.*, 1998; *Gurney et al.*, 2002].

[3] We concern ourselves in this paper with augmenting atmospheric inversions with information from the ocean. In the past, this has generally involved incorporating constraints from surface observations of the air-sea pCO_2 difference. Ocean constraints of this nature were first formally introduced into an atmospheric inversion by *Tans et al.* [1990]. As in previous studies [*Keeling et al.*, 1989; *Enting and Mansbridge*, 1989; *Tans et al.*, 1989], these authors sought to interpret atmospheric concentration gradients with the help of simulations of atmospheric transport and mechanistic models of surface processes. By also considering fluxes estimated from air-sea pCO_2 differences, they were able to make powerful arguments about the relative likelihoods of a collection of carbon source/sink scenarios. Among their conclusions was that the global ocean could not be removing more than 1 PgC yr^{-1} from the atmosphere in the period 1981–1987. Fitting the observed meridional gradient required a large sink in the northern temperate latitudes, a finding consistent with the

[1] Atmospheric and Oceanic Sciences Program, Princeton University, Princeton, New Jersey, USA.
[2] NOAA Earth System Research Laboratory, Boulder, Colorado, USA.
[3] Department of Atmospheric and Oceanic Sciences, University of California, Los Angeles, California, USA.
[4] Institute of Biogeochemistry and Pollutant Dynamics, ETH Zurich, Zurich, Switzerland.
[5] Earth and Biosphere Institute and School of Geography, University of Leeds, Leeds, UK.

0886-6236/07/2005GB002556$12.00

earlier conclusion of *Keeling et al.* [1989]. Unlike the study of *Keeling et al.* [1989], however, *Tans et al.* [1989] were able to attribute this sink to land on the basis of oceanic constraints, since observed air-sea pCO_2 differences in the extratropical northern oceans were too small to support an ocean sink of the required magnitude.

[4] Contemporary simulations of the ocean carbon cycle [e.g., *Siegenthaler*, 1983; *Sarmiento et al.*, 1992] were at odds with the ocean sink predictions of both of these inversion studies. The *Tans et al.* [1990] global ocean sink estimate was much smaller than simulations, and while *Keeling et al.* [1989] found a larger ocean sink, their attribution of the sink principally to the North Atlantic Ocean was not in agreement with model predictions and ΔpCO_2 observations. The dichotomy of interpretations of the ocean's role in the global carbon cycle has yet to be fully reconciled. Analyses of atmospheric oxygen and ^{13}C concentrations have generally supported a large ocean sink [*Keeling and Shertz*, 1992; *Battle et al.*, 2000; *Plattner et al.*, 2002; *Bopp et al.*, 2002], and a first inversion of ocean interior data [*Gloor et al.*, 2003] also found a larger ocean sink. Further inverse analyses of atmospheric CO_2 concentrations, however, have generally supported the existence of a smaller ocean sink [e.g., *Bousquet et al.*, 1999; *Gurney et al.*, 2002, 2004].

[5] In this paper, we couple an atmospheric CO_2 inversion to an inversion using ocean interior data. This "joint" inversion propagates information from the ocean to the land in a simple manner. Atmospheric inversions place strong constraints on surface fluxes aggregated in broad latitudinal bands, owing to the combination of strong zonal flow and sparse observations. Oceanic inversions, on the other hand, have the power to provide strong constraints on air-sea fluxes at higher spatial resolution, but do not directly address air-land fluxes. The estimated ocean fluxes indirectly constrain terrestrial fluxes by accounting for some of the total flux in the latitudinal bands. In this manner, flux estimates are obtained without regularization: we impose neither model-derived Bayesian priors, nor assumed correlations between regional fluxes.

2. Methods

[6] The joint inversion consists of transport inversions of atmospheric and oceanic observations, using multiple circulation models to assess the effects of errors in simulated transport. For each available model estimate of transport, we use the standard technique of weighted linear least squares to find the most probable fluxes to explain the available set of error-weighted observations [*Lawson and Hanson*, 1974]. Fluxes are estimated for 11 ocean and 11 land regions (Figure 1) as the annual mean over the period 1992–1996. In both the atmosphere and the ocean, the inversions interpret carbon observations using the "flux footprints" of the regions. For each region, this is the simulated steady state concentration field arising from the persistent unit flux of a passive dye tracer from the region. These unit responses, or Green's functions, are scaled until their summed contributions most closely match observed tracer concentrations. Final results include an estimate of the error due to transport uncertainty derived from the between-model differences in estimated fluxes. We first present the details of each of the component inversions, then describe how they are coupled to produce a jointly constrained estimate.

2.1. Atmospheric Inversion

[7] Atmospheric inversions are performed using the TransCom3, Level 1 (T3L1) transport estimates and atmospheric observational data set compiled from the NOAA Global Monitoring Division Globalview CO_2 data set [*GLOBALVIEW-CO$_2$*, 2000]. The methods used for the current atmospheric inversions follow those of T3L1 "control" inversion described by *Gurney et al.* [2002, 2003] exactly, with the exception of two modifications (detailed below). We have chosen to use the TransCom3 regional breakdown in order to exploit the model simulations performed for that experiment. The decision to use T3L1 simulations, observations, and error weights allows us to make direct comparisons between our results and those from that project without having to consider complications arising from methodological differences.

[8] Data to be inverted are the 1992–1996 average surface concentrations at 74 long-term monitoring stations. These long-term means comprise many individual samples. The choice of an annual mean estimation scheme is based on limitations of the oceanic inversions described later. As in the TransCom inversions, we exclude surface observations from the WITN surface and Darwin stations owing to concerns about data quality [*Gurney et al.*, 2003; *Law et al.*, 2003]. We use the standard weighted least-squares Green's function inversion, including observations (C_{obs}) and error estimates from T3L1. While these error estimates include the effects of measurement noise and biases, they are strongly influenced by assumed modeling errors. We make two modifications to the T3L1 inversion: prior flux estimates are not imposed, and the steady state atmospheric CO_2 "background" field generated by propagating *Takahashi et al.* [1999] (henceforth, Tak99)-estimated air-sea fluxes through each transport model (C_{Tak99}) is not presubtracted from the station observations. The detailed effects of these methodological changes on flux estimates are described in the auxiliary material of a companion paper [*Jacobson et al.*, 2007]. As in the T3L1 inversion, background CO_2 concentration fields resulting from estimates of the seasonal rectification of neutral land biosphere fluxes (C_{NBSR}) [*Denning et al.*, 1995] and fossil fuel fluxes (C_{FF}) are removed from the observations (C_{obs}) before inversion:

$$C_{anom} = C_{obs} - C_{NBSR} - C_{FF}. \quad (1)$$

The flux estimates resulting from this inversion of the anomalous concentration field (C_{anom}) implicitly include corrections to these assumed background flux fields in addition to fluxes from intentionally unmodeled processes such as land use change. Also as in T3L1, the sum of the flux estimates is constrained to agree with a mass-balance condition derived from an estimate of the difference between estimated fossil-fuel emissions for this period

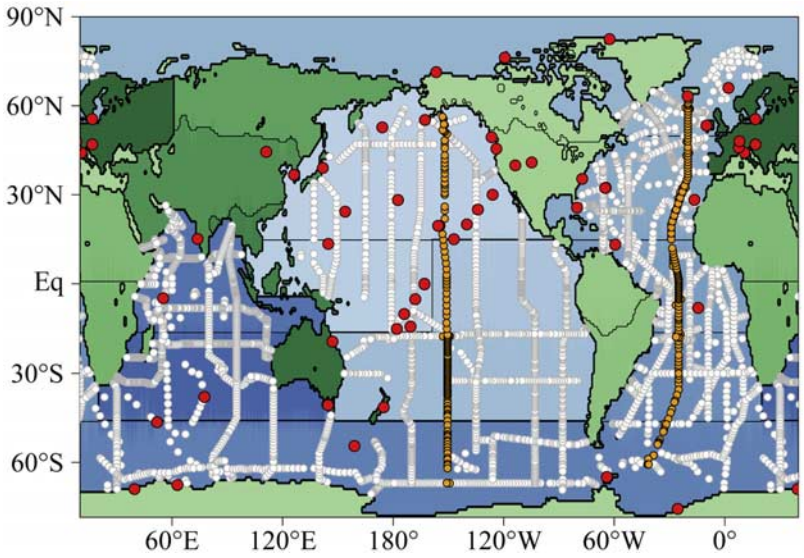

Figure 1. Flux regions and observational network. The 11 ocean regions (blue) and 11 land regions (green) are shown with locations of the 74 atmospheric stations (red) and 67,484 ocean observations (white). Oceanic stations along two meridional sections in the Atlantic and Pacific are highlighted in yellow; these sections will be discussed by *Jacobson et al.* [2007].

($\sim$6.1 PgC yr^{-1}) and the observed 1992–1996 atmospheric growth rate (3.3 ± 0.1 PgC yr^{-1}).

[9] The atmospheric inverse problem described here is ill-posed, with most regional fluxes poorly constrained by the available observations. Most inversion analyses use some form of regularization to attenuate the large uncertainties and unrealistically large best-guess fluxes that characterize raw inversion estimates. By avoiding regularization altogether, we admit large uncertainties in our results, especially for terrestrial flux estimates in the tropics and Southern Hemisphere. The uncertainties for poorly constrained regions are often strongly correlated with other regions, indicating that their flux estimates are interdependent. In contrast, regularization with Bayesian priors applied as independent regional estimates, that is, without prior between-region correlations, attenuates this error structure and makes the regional estimates appear to be more independent than data and transport simulations alone would predict. This effect is simply due to the application of priors as constraints on each region's flux independent of every other region. We take the position that preservation of the unregularized error structure is instructive. While many regions cannot be reasonably constrained individually, aggregating the interdependent regional flux estimates in postprocessing shows that large regions can still be constrained without introducing bias from model-derived priors or other regularization techniques. The raw errors from an unregularized inversion also give an objective assessment of the strength of data constraints. As detailed below, an independent motivation for this choice is that regional flux correlations are also the mechanism by which information from the ocean is propagated to terrestrial fluxes.

[10] Using annual mean station data for the atmospheric inversion requires the simulation of a land biosphere "rectifier" field [*Denning et al.*, 1995], which arises from the covariability of biospheric fluxes and atmospheric circulation. The requirement of simulating this field represents a potential source of bias in our results, as it involves the propagation of an assumed seasonal biospheric flux distribution through a model with a possibly incorrect simulation of seasonal variability in tropospheric circulation, with sensitivity to the representation of planetary boundary layer ventilation. Recent atmospheric inversion studies [e.g., *Baker*, 2001; *Gurney et al.*, 2002; *Rödenbeck et al.*, 2003b] have focused on analysis of monthly data to avoid this potential bias. This approach generally requires the estimation of monthly fluxes as well, however, and it remains to be shown that avoiding the potential bias of subtracting a simulated rectification effect is worth the cost of added dimensionality in the estimation problem. As described below, the ocean interior data used in this study are largely insensitive to variability with timescales less than about 5 years, so estimating annual mean fluxes is a natural choice.

[11] Seasonally varying air-sea fluxes in conjunction with seasonally varying atmospheric transport can also yield a rectifier effect. We have estimated the magnitude of this effect by propagating two sets of ocean inversion fluxes through the MOZART version 2 atmospheric transport model [*Horowitz et al.*, 2003] using interannually varying wind fields. In the first case, the air-sea fluxes are the monthly flux estimates from the oceanic inversion, with an global oceanic uptake of about 2 PgC yr^{-1}. In the second case, the fluxes are the annual mean of those inversion estimates. The difference between the atmospheric concentration response fields of these two simulations is analogous to the neutral land biosphere seasonal rectifier. We find that with the exception of specific locations in the atmosphere, the rectification signal is negligible. Surface volume mixing ratios of CO_2 averaged in the fourth year of simulation

sampled at the Transcom3 subset of GLOBALVIEW stations differ by no more than 3% between the two simulations, and 85% of the stations had a difference of less than 2%. The greatest differences were seen in the western subpolar regions of both the Pacific and Atlantic oceans, away from any GLOBALVIEW stations. For future studies employing observations over the oceans at latitudes between 40°N and 50°N, this rectification effect may need to be included.

2.2. Oceanic Inversion

[12] We use the ocean inversion method first elaborated by *Gloor et al.* [2003]. While our atmospheric and ocean inversions use a similar Green's function approach, there are three important differences that distinguish them. First and most important, the data density is much higher in the ocean than in the atmosphere. The ocean interior data come from 67,484 observations at stations distributed throughout the world ocean (Figure 1) and at which the entire vertical column is generally sampled. This allows us to estimate air-sea fluxes at fairly high resolution; fluxes are initially estimated for 27 oceanic regions with approximately twice the meridional resolution of the TransCom3 regions. The use of observations from the entire water column imposes an effective temporal smoothing on the data, since water below the mixed layer consists of contributions from multiple years that have been smoothed by mixing. Thus while the atmospheric data are time-averaged over the 1992–1996 period to remove their high-frequency components for the time-invariant atmospheric inversion, the ocean interior data are inherently suitable for investigations of processes with timescales of about 5 years and longer. The bulk of the data used in this study are available in the GLODAP version 1.0 [*Key et al.*, 2004] database, but some historical Atlantic data not present in the GLODAP product have also been used [*Mikaloff Fletcher et al.*, 2006].

[13] Secondly, the tracer concentrations being analyzed are not directly measured, but are the result of calculations designed to determine both that part of the oceanic dissolved inorganic carbon (DIC) distribution that is driven by the natural exchange of CO_2 across the air-sea interface, and the anthropogenic DIC concentration. While DIC concentrations at the surface are modified by air-sea exchange, away from the surface it is transformations related to biology that change DIC concentrations. The biological transformations include changes to and from both organic carbon and inorganic carbon in the form of $CaCO_3$. Considering for the moment only the organic carbon component, we can consider a potential DIC concentration that would result if phytoplankton were allowed to convert as much DIC to organic carbon as possible. In the absence of growth limitation by light or micronutrient availability and without remineralization opposing this process, photosynthetic production would proceed until all macronutrients were consumed. For this purpose, the availability of macronutrients is represented by observations of dissolved phosphate, so this potential reduction in DIC can be estimated by multiplying the observed PO_4^{-3} concentration by an assumed stoichiometric ratio of carbon to phosphate in organic material, $R_{C:P}$. The potential contribution of $CaCO_3$ formation to reducing DIC is more difficult to assess because Ca^{2+} concentrations in the ocean are largely insensitive to $CaCO_3$ formation and dissolution. Instead, the ocean's alkalinity (Alk), a measure of charge balance related to the carbon system, is used as an intermediary to infer the potential of hard-tissue formation to consume DIC. This contribution includes not only the observed alkalinity, but also a component of potential change in alkalinity due to consumption of NO_3^-, once more referenced to the phosphate concentration using a stoichiometric ratio, $R_{N:P}$. In the absence of anthropogenic carbon contamination, therefore, one can define a preindustrial carbon tracer that is conserved by assumption in the ocean interior,

$$\begin{aligned} C^*_{PI} &= DIC_{PI} - \Delta C_{bio} \\ &= DIC_{PI} - R_{C:P}\left[PO_4^{-3}\right] - \frac{1}{2}\left(Alk + R_{N:P}\left[PO_4^{-3}\right]\right), \end{aligned} \quad (2)$$

in which DIC_{PI} is the preindustrial in situ DIC concentration. In much of the world ocean, contemporary DIC has been increased over preindustrial levels owing to uptake of anthropogenic carbon from the atmosphere. To account for this perturbation, (2) is modified to yield a contemporary conserved tracer,

$$C^* = C^*_{PI} + C_{ant} = DIC - \Delta C_{bio}. \quad (3)$$

The anthropogenic carbon concentration, C_{ant}, is estimated using the ΔC^* method developed by *Gruber et al.* [1996]. For details of the computation of the anthropogenic carbon perturbation in the world ocean, the reader is referred to *Gruber* [1998] and *Sabine et al.* [1999, 2002]. Briefly, the ΔC^* method uses a Lagrangian approach in which the in situ C* value of a water parcel is differenced with the value that it is estimated to have had when it was last in contact with the atmosphere. Together, the C_{ant} manipulations require several assumptions, including that the stoichiometry of remineralization is known and constant, that the air-sea pCO_2 disequilibrium at any given location can be determined from available observations, that this disequilibrium has remained constant in time, and that the amount of time that has passed since the water was last at the surface can be estimated from CFC measurements. The recent manuscript of *Matsumoto and Gruber* [2005] presents a comprehensive analysis of potential biases due to these assumptions, and answers questions raised by *Hall et al.* [2004]. The implications of these biases and errors for the oceanic inversion are detailed later.

[14] Preindustrial gas exchange is estimated in the present work by analyzing the tracer

$$\begin{aligned} \Delta C_{gasex} &= C^* - C_{ant} - DIC^0 \\ &= DIC - \Delta C_{bio} - C_{ant} - DIC^0, \end{aligned} \quad (4)$$

which is simply C^*_{PI} reduced by an arbitrary constant DIC^0 chosen to make the average surface ΔC_{gasex} be nearly zero. In the limit that the anthropogenic and biological corrections are correct, variations in this tracer are due only to preindustrial gas exchange and mixing. Further details of this computation are described by *Gruber and Sarmiento*

Table 1. Circulation Characteristics, Inversion Fluxes, and Forward Simulation Fluxes of the MOM3 Model Simulations Used in This Study[a]

Title	Circulation Model Configuration Details	Watermass Transformation Rates, Sv			Preindustrial Flux Inverse Estimates, PgC/yr		1992–1996 Anthropogenic Flux Inverse Estimates, PgC/yr		Forward Simulations
		Southern Ocean	Low Latitude	NADW Formation	Takahashi CO_2	"Forward"	Takahashi CO_2	"Forward"	
LL	A_i low, K_v low	7.6	3.7	11.3	0.34	0.33	−1.94	−1.89	−1.90
HH	A_i high, K_v high	−12.5	24.5	12.0	0.35	0.47	−2.25	−2.24	−2.42
LHS	A_i low, K_v HiS	8.6	2.8	11.4	0.36	0.37	−2.03	−1.90	−2.04
P2A	A_i low, K_v med-HiS (2000 m), ECMWF, narrow Drake Passage	14.8	−2.0	12.8	0.42	0.46	−2.25	−2.06	−2.32
P2	A_i low, K_v med-HiS (2000 m), 4-pt enh. salinity restoring	6.8	5.4	12.2	0.34	0.41	−2.16	−2.07	−2.22
Average					0.39 ± 0.19[b]		−2.08 ± 0.14[b]		−2.18 ± 0.21

[a]Inversion estimates are presented for two different within-region flux patterns (see section 2.2). All five circulation configurations are constrained to have the same pycnocline structures and thus nearly equivalent North Atlantic deep water (NADW) formation rate [*Gnanadesikan and Hallberg*, 2000; *Gnanadesikan et al.*, 2004]. The models differ principally in how dense water is converted back to light water, with each one striking a different balance between processes in the Southern Ocean and in low latitudes. Conversion rates are estimated from the divergence of meridional transport of light ($\sigma_0 < 27.4$) waters. Forward simulations use the OCMIP2 "biotic" protocol [*Orr et al.*, 1999]. Preindustrial fluxes include 0.45 PgC yr^{-1} outgassing due to river carbon reaching the open ocean (see auxiliary material).
[b]For inverse estimates, value is average of Takahashi CO_2 and "Forward" flux patterns.

[2002], including a salinity normalization not discussed here. Representative fields of the ΔC_{gasex} and ΔC^* are given by *Jacobson et al.* [2007].

[15] The third major difference between atmospheric and oceanic inversions is that for the ocean data, we invert for preindustrial and anthropogenic carbon fluxes independently. The ocean estimation scheme inverts for steady state preindustrial fluxes and imposes smooth temporal variations on the anthropogenic fluxes [*Gloor et al.*, 2003; *Mikaloff Fletcher et al.*, 2006]. The preindustrial inversion involves running ocean dye tracers for footprint computations to quasi-steady state. The goal for these simulations is to have the dye concentration increasing everywhere at the same rate, and while this can never be perfectly achieved, we find that a reasonable approximation is obtained with 3,000 year integrations. The anthropogenic carbon inversion requires a further assumption due to the time-varying boundary condition of increasing atmospheric CO_2 concentration. It is observed that in forward simulations of the ocean carbon cycle, the anthropogenic air-sea flux is linearly related to the atmospheric CO_2 concentration throughout the 20th century. We use the simplifying assumption that anthropogenic fluxes are proportional to the smoothed atmospheric CO_2 perturbation. This approximation holds as long as the atmospheric CO_2 burden continues to grow at approximately the same exponential rate and the oceanic buffer capacity remains constant [*Sarmiento et al.*, 1995]. In the coming decades, this approximation will likely break down, but for the current data, collected between 1980 and 1998, the linearization of the ocean response is still a very good approximation. We have tested this assumption by comparing the flux estimated by this linearized response with the flux simulated by forward simulations of our suite of circulation models. Throughout the entire anthropogenic era, from 1765–1999, the global flux from the linear approximation deviates from forward simulations with a RMS error of 0.08 PgC yr^{-1}. For use in the joint inversion, we form a contemporary flux estimate, defined as the sum of preindustrial and anthropogenic (scaled to give the 1992–1996 mean) fluxes.

2.2.1. Transport, Errors, and Patterns

[16] The Green's function approach requires model simulations of the global "footprint" of flux into or out of each region. The eventual three-dimensional shape of a regional footprint is determined not only by advection and diffusion as simulated by the underlying general circulation model (GCM), but also by the spatial and temporal distribution of the unit of surface dye flux imposed on it. We assess uncertainty due to transport using a suite of configurations of the MOM3 ocean general circulation model [*Pacanowski and Gnanadesikan*, 1998]. This suite represents five different circulation schemes which vary on the basis of their vertical and along-isopycnal diffusivity coefficients, but maintain a density structure consistent with observations [*Gnanadesikan*, 1999; *Gnanadesikan et al.*, 2004]. The list of MOM3 configurations and their resultant forward and inverse estimates of global carbon flux are presented in Table 1. In this study we assess oceanic inversion uncertainty to the within-region spatial and temporal distribution of imposed surface dye flux by using two different schemes for each of the five circulation configurations. Atmospheric

inversion studies frequently use a single estimate of within-region flux pattern (but see *Gloor et al.* [1999] and *Rödenbeck et al.* [2003a]). Unlike the previous ocean inversion of *Gloor et al.* [2003], the surface flux patterns here include a seasonal cycle. Preindustrial and anthropogenic footprints are computed once for each model using the *Takahashi et al.* [2002] CO_2 flux patterns to partition the total annual regional flux into monthly contributions from each grid box. A second set of regional footprints is computed for each model using the monthly surface flux patterns manifested by that model in an OCMIP2 (Ocean Carbon Model Intercomparison Project 2) [*Orr et al.*, 2001] forward simulation. These latter patterns vary from model to model and have different preindustrial and anthropogenic patterns. In the *Takahashi et al.* [2002] surface flux pattern condition, the pattern is the same for each model and for the two eras.

[17] Assigned observational errors must account not only for uncertainty from random noise in the measurements, but also every other process that might contribute to the inability to perfectly invert fluxes. This includes systematic uncertainty due to errors in transport simulation, unmodeled processes affecting the observations, and various assumptions implicit in our inversion model. To account for all of these sources of error except the latter, a base observational uncertainty of 10 μmol kg^{-1} was assumed. To this value we add a spatially varying estimate of the uncertainty due to the use of fixed, but uncertain, stoichiometric ratios in the estimation of the biological contribution to observed DIC. Error estimates for stoichiometric uncertainty in C_{ant} were assigned following the scheme developed by *Mikaloff Fletcher et al.* [2006], based on an earlier analysis of O:C ratio sensitivity for the North Atlantic Ocean [*Gruber*, 1998]. In the *Mikaloff Fletcher et al.* [2006] scheme, errors are presumed to be a linear function of apparent oxygen utilization (AOU) and of C_{ant}. The ΔC_{gasex} tracer inherits all the uncertainty in C_{ant}, and has an additional component due to uncertainty in C:P stoichiometry. The results reported here were derived using a weighted least squares (WLS) error model, in which the observational errors vary in space, but are assumed to be independent from one another. The use of uncertain and spatially constant remineralization stoichiometry could lead to errors that are correlated between samples. To assess the effect of correlated errors on our estimates, a set of inversions was performed using generalized least squares, in which the off-diagonal elements of the observational error covariance matrix were determined using a Monte Carlo estimation of the error covariances. The results do not differ significantly from the WLS results reported here, and will not be discussed further. Representative values for the final observational uncertainties including the stoichiometric ratio contribution are about 30 μmol kg^{-1} for ΔC_{gasex} and about 20 μmol kg^{-1} for C_{ant}.

[18] Residuals from the regression fits are generally within 10 μmol kg^{-1} of zero for the anthropogenic case and 16 μmol kg^{-1} for the preindustrial case. We detected no significant lateral patterns in the residuals, but there are suggestions of coherent vertical variability. While anthropogenic residuals never differ significantly from zero, they generally have a maximum at around 500 meters depth. Residuals from the preindustrial inversion are also not significantly different from zero, and tend to have a mid-depth minimum at around 1000 m.

[19] Owing to the strong overdetermination of the oceanic flux estimation problem, the solution obtained is remarkably robust to assumptions made about the observational error model. To minimize biases due to estimating fluxes for large areas [*Kaminski et al.*, 2001], we initially estimated fluxes for a 27-region superset of the 11 TransCom3 ocean regions. These 27-region flux estimates are aggregated in postprocessing to the 11 TransCom3 regions for direct comparison with the atmospheric inversions. An important criterion in selecting the 27 regions was to avoid within-region flux heterogeneity, by considering features of the ocean circulation known to affect air-sea exchange such as frontal boundaries. Candidate regional selections were carefully compared with observed ΔpCO_2 variability and flux features from forward simulations in a further attempt to minimize within-region flux variability. Model simulations and ΔpCO_2-based flux estimates suggest that the spatial scales of air-sea flux variability in the open ocean are similar to the spatial extents of the 27 regions we have selected. The use of 27 regions instead of 11, coupled with our ability to minimize assumed within-region spatial flux variability, mitigates the potential for large region bias. At the same time, however, it is undeniable that there remains some risk of significant large region bias in our results, especially since the atmospheric component of our inversion retains the large regions of the TransCom inversion.

2.2.2. Relations With Other Ocean Inversions

[20] The current ocean inversions are related to a parallel set of inversions associated with the Ocean Inversion Project (OIP; see http://quercus.igpp. ucla.edu/OceanInversion/). The anthropogenic [*Mikaloff Fletcher et al.*, 2006] and preindustrial [*Mikaloff Fletcher et al.*, 2007] inversions from that project use the same C* data sets as the present work, but with slightly different error weighting schemes. In addition to the five simulations considered here, five other GCMs were available for the OIP inversions. While the OIP inversions sample a larger range of ocean transport uncertainty, the five simulations used here form a systematic exploration of a fundamental axis of transport uncertainty in coarse-resolution GCMs [*Gnanadesikan and Hallberg*, 2000; *Gnanadesikan et al.*, 2004]. Finally, the OIP simulations used one set of within-region surface flux patterns, whereas the simulations in this study used two different patterns. There is no indication at this time that OIP fluxes will differ significantly from the current oceanic inversion flux estimates.

2.3. Joint Inversion

[21] While the atmospheric inversion constrains fluxes into the atmosphere from both the land and sea, the oceanic inversion directly constrains only air-sea fluxes. We compute a jointly constrained surface flux estimate by combining information from atmospheric and oceanic inversions under the assumption that they provide independent estimates of air-sea fluxes.

[22] The issue of riverine carbon fluxes presents a potential inconsistency between the atmospheric and oceanic

inversions. As discussed in the online supplementary material, atmospheric inversions should in principle fully resolve the terrestrial and oceanic branches of the river carbon loop, whereas the present ocean inversions resolve only that portion of the cycle occurring in the open ocean. While the riverine component of the carbon cycle is poorly known [*Richey*, 2004], its inclusion is important for reconciling flux results from different methods [*Sarmiento and Sundquist*, 1992]. We adopt the perspective of an ideal atmospheric inversion for the purposes of this study. This requires that the ocean inversion estimates be corrected to account for an effective flux of riverine carbon to the open ocean, since this carbon is interpreted by the ocean inversion as an input across the air-sea interface. We estimate that after burial of organic and inorganic components in coastal sediments, about 0.45 PgC yr^{-1} reaches the open ocean. This riverine input, which masquerades in the oceanic inversion as a net air-sea CO_2 flux into the ocean, is resolved spatially and used to correct the ocean preindustrial flux estimate (see auxiliary material[1]).

[23] The estimate of fluxes from each atmospheric inversion is represented by a multivariate normal distribution, specified by a 22-element vector of mean values $\mathbf{x}_a$ and accompanying covariance matrix $\mathbf{P}a$. This is a result of error propagation of the assumed distribution of measurement errors through the matrix inverse. Our ordering convention places the air-land fluxes before the air-sea fluxes. In the joint inversion, the atmospheric flux estimates are updated with information from an oceanic inversion represented by an 11-element multivariate normal distribution ($\mathbf{x}_o$, $\mathbf{P}o$) to arrive at a joint estimate,

$$\mathbf{x}_j = \mathbf{x}_a + \mathbf{K}(\mathbf{x}_o - \mathbf{H}\mathbf{x}_a), \tag{5}$$

with covariance matrix

$$\mathbf{P}j = (\mathbf{I} - \mathbf{K}\mathbf{H})\mathbf{P}a, \tag{6}$$

in which $\mathbf{I}$ is the 22 × 22 identity matrix, and the observation kernel $\mathbf{H}$ is a matrix having dimension 11 rows by 22 columns. This matrix is all zeros with the exception of the diagonal of the right half, which is populated with ones. This structure represents the fact that the ocean inversions provide no direct constraint on terrestrial fluxes. $\mathbf{H}$ maps the parameters from the atmospheric inversion onto the parameters from the oceanic inversion, by extracting just the 11 air-sea fluxes from the 22-element atmospheric flux estimate. The update equation (5) is in the form of a "predictor-corrector" operation, and represents the Bayesian concept of combining a prior estimate ($\mathbf{x}_a$, $\mathbf{P}a$) from the atmospheric inversion with new information ($\mathbf{x}_o$, $\mathbf{P}o$) from the oceanic inversion.

[24] The "optimal gain matrix" $\mathbf{K}$ is determined using standard methods of sequential state estimation [*Kalman*, 1960; *Maybeck*, 1979],

$$\mathbf{K} = \mathbf{P}a\mathbf{H}^{\mathrm{T}}\left(\mathbf{H}\mathbf{P}a\mathbf{H}^{\mathrm{T}} + \mathbf{P}o\right)^{-1}, \tag{7}$$

in which $(\ )^{\mathrm{T}}$ and $(\ )^{-1}$ are the matrix transpose and inverse, respectively.

[25] To provide some insight into manipulations represented by (5) to (7), it is instructive to consider the hypothetical situation in which the oceanic inversion provides direct estimates of air-land fluxes in addition to air-sea fluxes. In this case $\mathbf{H}$ would be the 22 × 22 identity matrix, and $\mathbf{K}$ would be the multidimensional generalization of the ratio of variances of atmospheric uncertainty to the sum of atmospheric and oceanic uncertainty. We consider the limiting cases in which the atmospheric and oceanic variances have very different magnitudes. If the oceanic uncertainty $\mathbf{P}o$ were much greater than the atmospheric uncertainty, the gain $\mathbf{K}$ would tend to have small values. Via (5), $\mathbf{x}_j$ would thus be little changed from $\mathbf{x}_a$, and via (6), $\mathbf{P}j$ would be similarly unaffected. In contrast, as $\mathbf{P}o$ becomes much smaller than $\mathbf{P}a$, $\mathbf{K}$ tends to the identity matrix. In this limiting case, the oceanic information dominates: (5) yields a final estimate $\mathbf{x}_j \sim \mathbf{x}_o$, and the final uncertainty $\mathbf{P}j$ becomes correspondingly small.

[26] In the atmosphere, there are 16 transport models and thus 16 different estimates of surface fluxes; in the ocean we use 10 different transport simulations and flux estimates. We take the position that a reasonable sample of the total probability distribution is to consider the entire set of 160 permutations. Transport uncertainty is considered before performing the coupling for each pairwise atmospheric model-oceanic model permutation. The uncertainty $\mathbf{P}a$ represents not only the propagation of assumed observational errors through an individual atmospheric inversion ("internal" or "within-model" error, $\mathbf{P}a^{\mathrm{Int}}$), but also includes a component due to across-model transport ("external") uncertainty $\mathbf{P}a^{\mathrm{Ext}}$,

$$\mathbf{P}a = \mathbf{P}a^{\mathrm{Int}} + \mathbf{P}a^{\mathrm{Ext}}. \tag{8}$$

The across-model uncertainty is estimated by forming a covariance matrix from the central values of the 16 available flux estimates,

$$\mathbf{P}a^{\mathrm{Ext}} = \mathrm{cov}\left(\mathbf{x}_{a,i}\right), \quad i = 1 \ldots 16. \tag{9}$$

Likewise, $\mathbf{P}o$ includes a sample estimate of transport uncertainty from the 10 available ocean simulations. These across-model uncertainties are sample estimates of the total transport uncertainty, and could be significantly biased owing to models having similar deficiencies. This is a source of potential error that we cannot formally quantify with the current method.

[27] Whereas within-model uncertainty is more important for the present atmospheric inversions, the ocean inversions are dominated by across-model uncertainty. The sparse spatial distribution of data in the atmosphere yields high internal uncertainties for unregularized atmospheric inversions, so that intermodel differences in transport have little statistical significance. The oceanic inversions, on the other hand, are strongly overdetermined by the large number of observations, which drives down the internal error estimates to very low levels. This allows the across-model component of uncertainty to become more evident in the ocean inver-

[1] Auxiliary materials are available at ftp://ftp.agu.org/apend/gb/2005gb002556.

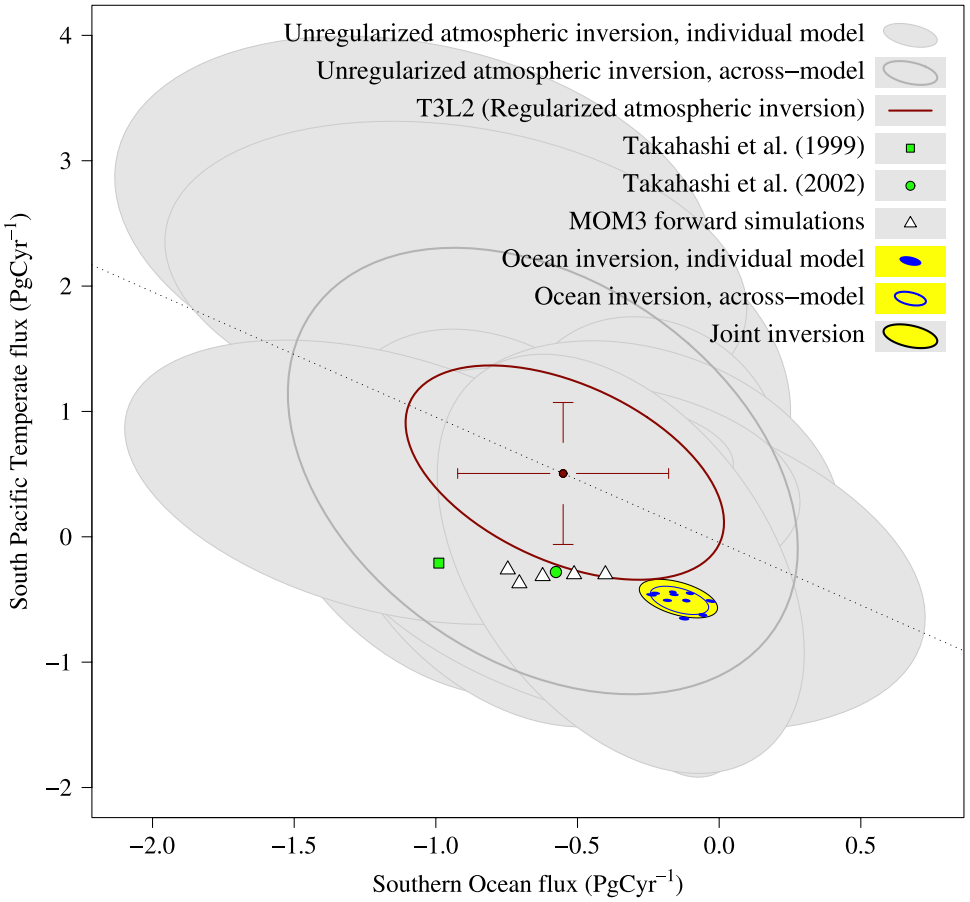

Figure 2. Construction of the joint inverse, using the example of 1992–1996 flux estimates for the Southern Ocean and South Pacific Temperate regions. The 68% confidence interval for each estimate is shown as an error ellipsoid, for which a leftward tilt indicates anticorrelation between the two regional estimates. The more that the tilt approaches a slope of −1 (dotted line) and the ellipse narrows, the less power an inversion has to discriminate between the regions. Individual unregularized atmospheric inversions are shaded in light grey and their across-model summary is the dark grey unfilled ellipse. TransCom3 Level 2 (T3L2) results [*Gurney et al.*, 2004], combining both within- and across-model uncertainty in quadrature, are shown as red error bars (reported) of one standard deviation and as a red ellipse (reproduced). It is a general feature of the multivariate normal distribution that the ±1 standard deviation error bars appears smaller than the corresponding dimension of the 68% confidence interval error ellipse. Individual ocean inversion results are shown as blue filled ellipses, and their across-model summary is the blue unfilled ellipse. The final joint inversion result is the yellow ellipse with a black border. For comparison, *Takahashi et al.* [1999] estimates for 1995 are shown with a green square, and *Takahashi et al.* [2002] 1995 estimates are shown with a green circle. Fluxes from forward simulations of the MOM3 suite are depicted by white triangles.

sion. The relative roles of the errors from the two inversions are highlighted in Figure 2, in which confidence intervals for the unregularized atmospheric inversion estimates of air-sea flux (in gray) are large and overlapping, whereas those for the oceanic inversions (in blue) are much smaller and well-separated from one another.

3. Discussion

[28] The yellow ellipse in Figure 2 represents the 68% confidence interval for the air-sea fluxes in the Southern Ocean and South Pacific Temperate regions. This estimate is formally inconsistent with forward simulations made using the same circulation configurations of the MOM3 ocean GCM, and with flux estimates derived from the surface ΔpCO_2 climatology of *Takahashi et al.* [1999, 2002]. While the joint inversion flux estimate is also inconsistent with the regularized atmospheric inversion of *Gurney et al.* [2004], it is not in disagreement with the unregularized atmospheric estimates from the present study, as shown by the overlap of the yellow and gray ellipses. The joint inversion suggests that the Southern Ocean south of

Table 2. Summary of Global Estimates of Air-Land and Air-Sea Fluxes[a]

Source	Global Air-Land Flux	Global Air-Sea Flux		
		Anthropogenic Φ_{anthro}	Preindustrial $\Phi_{preindust}$	Contemporary $\Phi_{contemp}$
IPCC TAR	-1.4 ± 0.7[b]			-1.7 ± 0.5[b,c]
T3L1	-1.3 ± 1.4			-1.5 ± 1.4
T3L2	-1.5 ± 1.0			-1.3 ± 1.0
Bopp O_2/N_2	-1.7 ± 0.9[d,e] (-1.2 ± 0.9)[d]			-1.9 ± 0.9[c,e] (-2.3 ± 0.7)[d]
Keeling O_2/N_2	-1.7 ± 0.8[b,e] (-1.3 ± 0.8)[b]			-1.4 ± 0.6[c,e] (-1.9 ± 0.6)[b]
Joint	-1.1 ± 0.2	-2.1 ± 0.1	0.4 ± 0.2[e]	-1.7 ± 0.2
Gloor inverse		-1.9 ± 0.3 (-1.7 ± 0.3)[c,f]	0.4 ± 0.3[e]	-1.5 ± 0.4 (-1.8 ± 0.4)[c,e,f]
McNeil CFCs				-1.5 ± 0.4 (-2.0 ± 0.4)[b,c,e]
Matsumoto OCMIP				-1.7 ± 0.2 (-2.2 ± 0.2)[b,c,e]
Tak99 $k \sim u^2$				2.1[b]
Tak02 $k \sim u^2$				1.6[b]
Tak02 $k \sim u^3$				2.3[b]
MOM3 forward		-2.2 ± 0.2	0.4 ± 0.1[e]	-1.7 ± 0.2[e]

[a]Estimates have been corrected so that river carbon flow is manifested as a land sink and a preindustrial ocean source of 0.45 PgC yr^{-1} (see auxiliary material). Contemporary air-sea fluxes ($\Phi_{contemp} = \Phi_{preindust} + \Phi_{anthro}$) have been scaled to the 1992–1996 period by assuming the anthropogenic component is proportional to the atmospheric concentration perturbation, but air-land fluxes are not scaled. Original estimates, uncorrected for river carbon and unscaled in time, are given in parentheses. "IPCC-TAR 90s" is the estimate of *Prentice et al.* [2001] for the 1990s; "T3L1" and "T3L2" are the TransCom3 control inversions for level 1 [*Gurney et al.*, 2002] and level 2 [*Gurney et al.*, 2004], respectively, both for the period 1992–1996. "Bopp O_2/N_2" and "Keeling O_2/N_2" represent the oxygen analyses of *Bopp et al.* [2002] for the period 1990–1996 and *Keeling and Garcia* [2002] for the 1990s, respectively. "Joint" is the current joint inversion for the period 1992–1996. "Gloor inverse" is the previous ocean inversion of *Gloor et al.* [2003] scaled to 1992–1996, a result nearly identical to that of *McNeil et al.* [2003] from CFC analysis. "Matsumoto OCMIP" is the summary of forward ocean carbon cycle simulations [*Orr et al.*, 2001], as reported by *Matsumoto et al.* [2004], also scaled to 1992–1996. "Tak99" and "Tak02" represent estimates based on the ΔpCO_2 analyses of *Takahashi et al.* [1999, 2002] respectively, using quadratic ("$k \sim u^2$" [*Wanninkhof*, 1992]) and cubic ("$k \sim u^3$" [*Wanninkhof and McGillis*, 1999]) gas transfer velocity parameterizations. "MOM3 Forward" are the 1992–1996 fluxes from OCMIP2 biotic simulations for the five models of the MOM3 suite used in the present study (see Table 1 of *Jacobson et al.* [2007]).

[b]For the period of the 1990s.

[c]Air-sea fluxes scaled to 1992–1996 by assuming that the anthropogenic flux is proportional to the atmospheric CO_2 perturbation.

[d]For the period 1990–1996.

[e]Includes 0.45 ± 0.18 PgC yr^{-1} to account for river carbon fluxes (see auxiliary material).

[f]For the period 1990–1991.

44°S is a negligible net sink of carbon, whereas the extratropical South Pacific Ocean is a significant net sink.

[29] The formal uncertainties in air-sea fluxes estimated by the oceanic inversions are so much smaller than the corresponding values from the atmospheric inversions that their coupling is effectively equivalent to using the ocean inversion estimates as fixed ocean priors in an atmospheric inversion, although it is important to retain the full uncertainty covariance matrix for this ocean prior. While atmospheric inversions have a negligible impact on the final air-sea flux estimates, information flows from the ocean to the land, via correlations in flux estimates from the atmospheric inverse. Since these correlations in the atmospheric estimate are the direct mathematical means by which the ocean informs terrestrial fluxes, it is important to understand their causes. Owing to vigorous zonal mixing in the atmosphere and a sparse observational data set, atmospheric inversions have difficulty partitioning fluxes within broad regional bands into contributions from the continents and basins within each such band. This effect manifests itself as large off-diagonal elements in the covariance matrix of parameter uncertainty linking such neighboring areas, indicating that the flux estimates are significantly correlated. The mass balance constraint used in the atmospheric inversion induces further correlations between flux estimates since it imposes a condition on the sum of all the fluxes. Ocean inversions, on the other hand, provide strong constraints on the air-sea component within these bands whose individual regions are poorly resolved by the atmospheric inversion. By accounting for the ocean portion of the total flux, we can estimate the residual terrestrial flux with greater certainty.

3.1. Effects of the Ocean Constraint on Flux Estimates

[30] Considering oceanic and atmospheric observations in a joint inversion framework provides several unique insights into the global carbon cycle. Flux estimates over both land and ocean regions show significant differences from previous inversions and other estimates (Table 2). As discussed above, we chose to use atmospheric inversions similar to those of *Gurney et al.* [2002], (T3L1) not only to benefit from the suite of atmospheric transport simulations performed for the TransCom3 experiment, but also to aid the interpretation of our results by allowing direct comparison with that benchmark study. Our estimate differs from the T3L1 results mainly owing to two factors: (1) the avoidance of model-based priors and (2) the use of air-sea fluxes from ocean interior data. These effects are detailed in the online supplementary material of *Jacobson et al.* [2007]. We depict in Figure 3 the combined effects of these two factors on air-sea and air-land flux estimates by drawing a line segment for each flux region on a two-dimensional space of flux magnitude versus uncertainty. The starting point for each line segment is an estimate from an atmosphere-only inversion using priors (similar to T3L1), and the ending point, shown with a colored plot symbol, is the joint inversion estimate. Whether a given result can be statistically distinguished from zero depends on how many standard deviations away it is from zero (gray shaded isopleths).

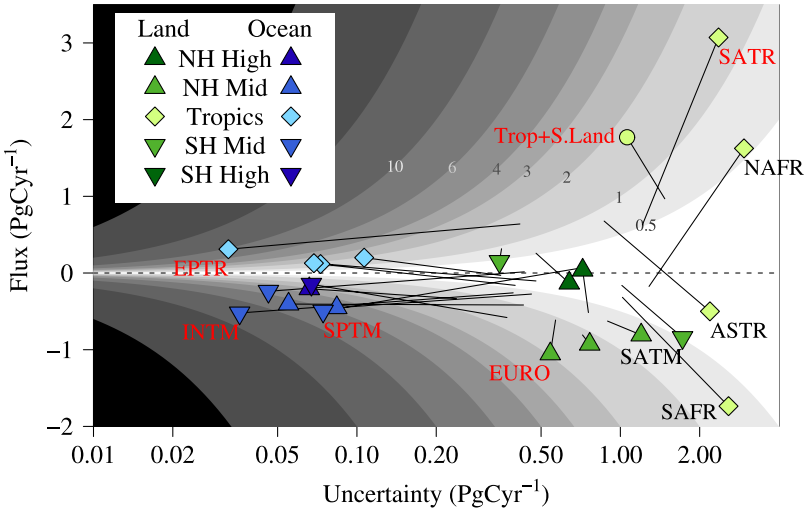

Figure 3. Effect of the ocean constraint on regional estimates of annual-mean surface flux of CO_2 in PgC yr^{-1}. Each line segment shows the change from the atmosphere-only TransCom3, Level 1 control inversion with priors (end of line without a plot symbol) to joint ocean-atmosphere inversion estimates without priors (end with a plot symbol). Estimated fluxes are on the vertical axis and uncertainties (1 s.d.) are plotted with a log scale on the horizontal axis. Air-sea fluxes have a blue plot symbol, and air-land fluxes are in green, with the shape and color shade giving the latitude band of the flux region, as shown in the key. The aggregate of land regions in the tropics and Southern Hemisphere ("Trop + S.Land") is shown using a light green circular plot symbol. Isopleths of statistical significance (the number of standard deviations away from zero) are shaded in gray. Names (see Table 1 of *Jacobson et al.* [2007]) are shown for selected regions, with those in red having joint inversion estimates that are significantly different than zero.

[31] Figure 3 shows that as expected, the use of ocean interior data drives uncertainty in our estimate of air-sea fluxes to low values, with no ocean region having an uncertainty of more than about 0.1 PgC yr^{-1}. All air-sea flux estimates are significantly different from zero owing to these low uncertainties. Tropical regions (light blue diamonds) are all sources, and southern temperate latitudes are the strongest sinks (downward pointing medium blue triangles). The high-latitude oceans of both hemispheres (darkest blue triangles) are weak sinks.

[32] While temperate land regions (medium green triangles in Figure 3) are generally significant sinks, boreal zones (darkest green triangles) are found to be more neutral. The joint inversion has in all cases larger flux uncertainties for individual terrestrial regions than the T3L1 inversion, since we do not use prior estimates to regularize the solution. The line segments corresponding to land regions in Figure 3 all terminate with plot symbols further to the right than their starting points. This effect is much stronger for tropical land regions (light green diamonds) than for mid- and high-latitude land regions. While the estimates and accompanying uncertainties for tropical land regions undergo strong changes, the corresponding changes in significance level, measured as the number of standard deviations that a given result is away from zero (gray-shaded isopleths), are much smaller. For instance, while the uncertainty of the tropical South American flux (SATR) nearly doubles from T3L1 to the joint estimate, its significance actually increases, from 0.5 to 1.3 standard deviations away from zero. The T3L1 result can be distinguished from zero with a 70% probability, but the joint inversion estimate is more statistically significant, indicating with a 90% probability that the South American tropics are a source of carbon to the atmosphere. Terrestrial flux estimates from the joint inversion, and especially aggregates fluxes for several regions considered together, are analyzed in detail in a companion paper [*Jacobson et al.*, 2007]. The auxiliary material of that paper also discusses the effects of each of the methodological changes that distinguish the T3L1 inversion from the current unregularized atmospheric and joint inversions.

3.2. Land-Ocean Partitioning of the Total Sink

[33] The joint inversion estimate of 1992–1996 average annual uptake of carbon dioxide by the land and ocean combined is 2.8 ± 0.1 PgC yr^{-1}, in agreement with TransCom 3, Level 1 and Level 2 (henceforth, T3L1 and T3L2, respectively), owing to the use of a similar mass balance constraint. The partitioning of this global flux between terrestrial and oceanic components is similar, although the uncertainties on the global fluxes are significantly reduced. The joint inversion indicates that air-sea flux is responsible for 60% of the total uptake (lower three rows of Table 1 of *Jacobson et al.* [2007]). The anthropogenic air-sea flux of carbon, is estimated to be −2.1 ± ~0.2 PgC yr^{-1}, similar to that estimated by *Mikaloff Fletcher et al.* [2006]. While the spatial distribution of terrestrial flux is still subject to significant uncertainty, the confidence we have on the

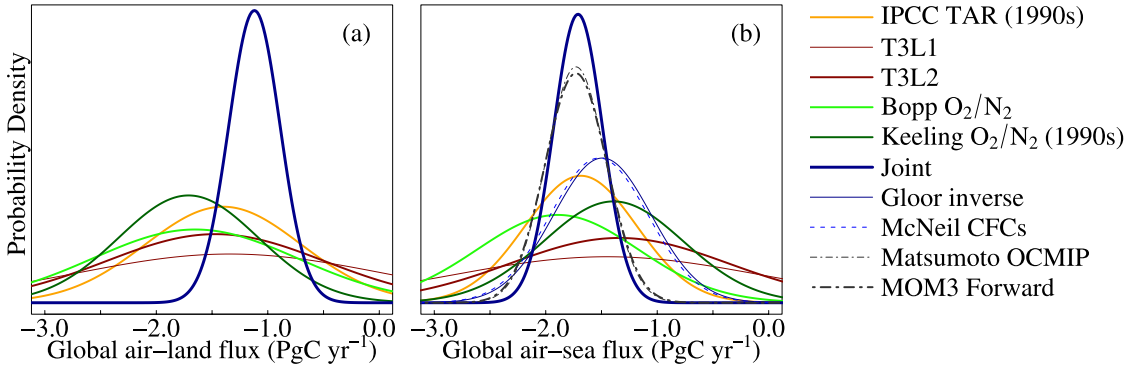

Figure 4. Probability density distributions for the partitioning of the total atmospheric sink into (a) terrestrial and (b) oceanic components, according to various reports in the literature, assuming normal distributions. Estimates have been corrected such that the riverine carbon loop appears as a land sink and an ocean source of 0.45 PgC yr^{-1} (see auxiliary material), and air-sea fluxes have been scaled to the 1992–1996 period. For corrections, scaling, and references, see Table 2.

atmospheric growth rate and on the total air-sea flux allows the joint inversion to determine the total land flux with a high degree of confidence (Figure 4). These reported uncertainties comprise only those sources of error that are formally quantifiable, and actual uncertainties are probably higher.

[34] Atmospheric oxygen and ^{13}C analyses [*Battle et al.*, 2000; *Keeling and Garcia*, 2002] and pCO_2-based flux estimates [*Takahashi et al.*, 2002] agree that the ocean is a larger sink for anthropogenic carbon than is the land (Table 2 and Figure 4). Forward simulations of the ocean carbon cycle [*Orr et al.*, 2001; *Matsumoto et al.*, 2004; *Jacobson et al.*, 2007, Table 1] predict an even greater ocean sink of anthropogenic carbon. The atmospheric inversions of TransCom Level 1 [*Gurney et al.*, 2002] and Level 2 [*Gurney et al.*, 2004], and of [*Rödenbeck et al.*, 2003a] have a more balanced partitioning between land and ocean sinks. (Note however that *Rödenbeck et al.* [2003a] state that their results are suited for analysis of temporal variability and may not be appropriate for studies of long-term averages.)

4. Conclusions

[35] We have coupled independent inversions in the atmosphere and the ocean to produce a jointly constrained estimate of surface fluxes of carbon dioxide in the period 1992–1996. The linear combination of these two inversions yields an estimate which is consistent with CO_2 mixing ratios in the atmosphere from the NOAA ESRL/GMD cooperative observational network, and with ocean interior measurements from the GLODAP ocean carbon data analysis project. Air-sea fluxes from the oceanic inversion have relatively small uncertainties, and provide a powerful constraint for the analysis of atmospheric observations. This has allowed us to refrain from using model-based priors to regularize the flux estimate, while still obtaining reasonable uncertainties for individual land regions in the well-observed Northern Hemisphere.

[36] The net oceanic carbon sink averaged over the 1992–1996 period was responsible for an air-sea flux of -1.7 ± 0.2 PgC yr^{-1}, comprising an anthropogenic flux of -2.1 ± 0.2 PgC yr^{-1} imposed on a natural background outgassing of 0.4 ± 0.2 PgC yr^{-1}. These estimates are strongly constrained by the data coverage in the recently completed oceanic carbon survey [*Key et al.*, 2004]. The uncertainty on this estimate formally includes components due to biogeochemical assumptions, transport biases, uncertainty in poorly known river carbon fluxes, and measurement errors. Its low value is driven by the large number of locations at which ocean interior data are available, and by the relatively well-distributed three-dimensional sampling in the ocean. It is, however, only a formal error estimate, including only those sources of errors that we could quantify. Actual errors are likely to be larger.

[37] The terrestrial sink we predict (-1.1 ± 0.2 PgC yr^{-1}) is generally smaller than predicted by analyses of atmospheric oxygen and inversions of atmospheric CO_2, but uncertainty levels in those estimates are too high to make claims of a significant difference.

[38] Flux estimates from tropical and southern land regions are poorly constrained by this method, but some significance levels are increased. Notably, despite a large uncertainty, the South American tropics are found to be a net source of carbon to the atmosphere. This is discussed in detail in a companion manuscript [*Jacobson et al.*, 2007].

[39] **Acknowledgments.** Jacobson, Sarmiento, and Gloor were supported by an award from the National Oceanic and Atmospheric Administration, U.S. Department of Commerce, and by the Carbon Mitigation Initiative, with support provided by BP Amoco and the Ford Motor Company. Gruber and Mikaloff Fletcher were supported by a grant from the National Aeronautics and Space Administration. The present analysis would not be possible without the observational data provided by countless oceanographers participating in the WOCE/JGOFS campaign and atmospheric scientists participating in the Globalview-CO_2 program. We thank Steve Pacala, Robbie Toggweiler, and five anonymous reviewers for helpful suggestions on an earlier draft of this paper. TransCom modelers are K. R. Gurney, R. M. Law, A. S. Denning, P. J. Rayner, D. Baker, P. Bousquet, L. Bruhwiler, Y.-H. Chen, P. Ciais, S.-M. Fan, I. Fung, M. Gloor, M. Heimann, K. Higuchi, J. John, T. Maki, S. Maksyutov, P. Peylin, M. Prather, B. C. Pak,

J. L. Sarmiento, S. Taguchi, T. Takahashi, and C.-W. Yuen. TransCom results were made possible through support from the National Science Foundation (OCE-9900310), the National Oceanic and Atmospheric Administration (NA67RJ0152, Amend 30) and the International Geosphere Biosphere Program/Global Analysis, Interpretation, and Modeling Project. The statements, findings, conclusions, and recommendations are those of the authors and do not necessarily reflect the views of the National Oceanic and Atmospheric Administration, or the U.S. Department of Commerce.

References

Amiotte-Suchet, P., and J.-L. Probst (1995), A global model for present day atmospheric/soil CO_2 consumption by chemical erosion of continental rocks (GEM-CO_2), *Tellus, Ser. B*, *47*, 273–280.

Aumont, O., J. C. Orr, P. Monfray, W. Ludwig, P. Amiotte-Suchet, and J. L. Probst (2001), Riverine-driven interhemispheric transport of carbon, *Global Biogeochem. Cycles*, *15*(2), 393–405.

Baker, D. F. (2001), Sources and sinks of atmospheric CO_2 estimated from batch least-squares inversions of CO_2 concentration measurements, Ph.D. thesis, Princeton Univ., Princeton, N. J.

Battle, M., M. L. Bender, P. P. Tans, J. W. C. White, J. T. Ellis, T. Conway, and R. J. Francey (2000), Global carbon sinks and their variability inferred from atmospheric O_2 and $\delta^{13}C$, *Science*, *287*, 2467–2470.

Bolin, B., and C. D. Keeling (1963), Large-scale atmospheric mixing as deduced from seasonal and meridional variations of carbon dioxide, *J. Geophys. Res.*, *68*(13), 3899–3920.

Bopp, L., C. LeQuéré, M. Heimann, A. C. Manning, and P. Monfray (2002), Climate-induced oxygen oceanic fluxes: Implications for the contemporary carbon budget, *Global Biogeochem. Cycles*, *16*(2), 1022, doi:10.1029/2001GB001445.

Bousquet, P., P. Ciais, P. Peylin, M. Ramonet, and P. Monfray (1999), Inverse modeling of annual atmospheric CO_2 sources and sinks: 1. Method and control inversion, *J. Geophys. Res.*, *104*(D21), 26,161–26,178.

Chen, C.-T. A. (2004), Exchanges of carbon in the coastal seas, in *The Global Carbon Cycle: Integrating Humans, Climate, and the Natural World*, edited by C. B. Field and M. R. Raupach, pp. 341–351, Island, Washington.

Compton, J., D. Mallinson, C. Glenn, G. Filippelli, K. Föllmi, G. Shields, and Y. Zanin (2000), Variations in the global phosphorous cycle, in *Marine Authigenesis: From Global to Microbial*, pp. 21–33, Soc. for Sed. Geol. (SEPM), Tulsa, Okla.

Denning, A. S., I. Y. Fung, and D. Randall (1995), Latitudinal gradient of atmospheric CO_2 due to seasonal exchange with land biota, *Nature*, *376*, 240–243.

Enting, I., and J. Mansbridge (1989), Seasonal sources and sinks of atmospheric CO_2: Direct inversion of filtered data, *Tellus, Ser. B*, *41*, 111–126.

Fan, S.-M., M. Gloor, J. Mahlman, S. Pacala, J. L. Sarmiento, T. Takahashi, and P. Tans (1998), A large terrestrial carbon sink in North America implied by atmospheric and oceanic carbon dioxide data and models, *Science*, *282*, 442–446.

GLOBALVIEW-CO_2 (2000), Cooperative Atmospheric Data Integration Project—Carbon Dioxide, Natl. Oceanic and Atmos. Admin., Boulder, Colo.

Gloor, M., S.-M. Fan, S. Pacala, J. L. Sarmiento, and M. Ramonet (1999), A model-based evaluation of inversions of atmospheric transport, using annual mean mixing ratios, as a tool to monitor fluxes of nonreactive trace substances like CO_2 on a continental scale, *J. Geophys. Res.*, *104*(D12), 14,245–14,260.

Gloor, M., N. Gruber, J. Sarmiento, C. L. Sabine, R. A. Feely, and C. Rödenbeck (2003), A first estimate of present and preindustrial air-sea CO_2 flux patterns based on ocean interior carbon measurements and models, *Geophys. Res. Lett.*, *30*(1), 1010, doi:10.1029/2002GL015594.

Gnanadesikan, A. (1999), A simple predictive model for the structure of the oceanic pycnocline, *Science*, *283*, 2077–2079.

Gnanadesikan, A., and R. W. Hallberg (2000), On the relationship of the circumpolar current to Southern Hemisphere winds in coarse-resolution ocean models, *J. Phys. Oceanogr.*, *30*, 2013–2034.

Gnanadesikan, A., J. P. Dunne, R. M. Key, K. Matsumoto, J. L. Sarmiento, R. D. Slater, and P. S. Swathi (2004), Oceanic ventilation and biogeochemical cycling: Understanding the physical mechanisms that produce realistic distributions of tracers and productivity, *Global Biogeochem. Cycles*, *18*(4), GB4010, doi:10.1029/2003GB002097.

Gruber, N. (1998), Anthropogenic CO_2 in the Atlantic Ocean, *Global Biogeochem. Cycles*, *12*(1), 165–191.

Gruber, N., and J. L. Sarmiento (2002), Large-scale biogeochemical-physical interactions in elemental cycles, in *The Sea*, pp. 337–399, John Wiley, Hoboken, N. J.

Gruber, N., J. L. Sarmiento, and T. F. Stocker (1996), An improved method for detecting anthropogenic CO_2 in the oceans, *Global Biogeochem. Cycles*, *10*(4), 809–837.

Gurney, K. R., et al. (2002), Towards robust regional estimates of CO_2 sources and sinks using atmospheric transport models, *Nature*, *415*, 626–630.

Gurney, K. R., et al. (2003), TransCom 3 CO_2 inversion intercomparison: 1. Annual mean control results and sensitivity to transport and prior flux information, *Tellus, Ser. B*, *55*, 555–579.

Gurney, K. R., et al. (2004), Transcom 3 inversion intercomparison: Model mean results for the estimation of seasonal carbon sources and sinks, *Global Biogeochem. Cycles*, *18*(1), GB1010, doi:10.1029/2003GB002111.

Hall, T. M., D. W. Waugh, T. W. N. Haine, P. E. Robbins, and S. Khatiwala (2004), Estimates of anthropogenic carbon in the Indian Ocean with allowance for mixing and time-varying air-sea CO_2 disequilibrium, *Global Biogeochem. Cycles*, *18*(1), GB1031, doi:10.1029/2003GB002120.

Hedges, J. I., and R. G. Keil (1995), Sedimentary organic-matter preservation—An assessment and speculative synthesis, *Mar. Chem.*, *49*(2–3), 81–115.

Horowitz, L. W., et al. (2003), A global simulation of tropospheric ozone and related tracers: Description and evaluation of MOZART, version 2, *J. Geophys. Res.*, *108*(D24), 4784, doi:10.1029/2002JD002853.

Jacobson, A. R., J. L. Sarmiento, M. Gloor, N. Gruber, and S. E. Mikaloff Fletcher (2007), A joint atmosphere-ocean inversion for surface fluxes of carbon dioxide: 2. Regional results, *Global Biogeochem. Cycles*, *21*, GB1020, doi:10.1029/2006GB002703.

Kalman, R. E. (1960), A new approach to linear filtering and prediction problems, *J. Basic Eng.*, *82D*, 35–45.

Kaminski, T., P. J. Rayner, M. Heimann, and I. G. Enting (2001), On aggregation errors in atmospheric transport inversions, *J. Geophys. Res.*, *106*(D5), 4703–4715.

Keeling, C. D. (1960), The concentration and isotopic abundances of carbon dioxide in the atmosphere, *Tellus*, *12*, 200–203.

Keeling, C., S. Piper, and M. Heimann (1989), A three-dimensional model of atmospheric CO_2 transport based on observed winds: 4. Mean annual gradients and interannual variations, in *Aspects of Climate Variability in the Pacific and the Western Americas*, *Geophys. Monogr. Ser.*, vol. 55, edited by D. Peterson, AGU, Washington, D. C.

Keeling, R. F., and H. E. Garcia (2002), The change in oceanic O_2 inventory associated with recent global warming, *Proc. Natl. Acad. Sci. U. S. A.*, *99*(12), 7848–7853.

Keeling, R. F., and S. R. Shertz (1992), Seasonal and interannual variations in atmospheric oxygen and implications for the global carbon cycle, *Nature*, *358*, 723–727.

Key, R. M., et al. (2004), A global ocean carbon climatology: Results from Global Data Analysis Project (GLODAP), *Global Biogeochem. Cycles*, *18*, GB4031, doi:10.1029/2004GB002247.

Law, R. M., Y.-H. Chen, K. R. Gurney, and TransCom 3 Modellers (2003), TransCom 3 CO_2 inversion intercomparison: 2. Sensitivity of annual mean results to data choices, *Tellus, Ser. B*, *55*, 580–595.

Lawson, C. L., and R. J. Hanson (1974), *Solving Least Squares Problems*, Prentice-Hall, Upper Saddle River, N. J.

Ludwig, W., J. L. Probst, and S. Kempe (1996), Predicting the oceanic input of organic carbon by continental erosion, *Global Biogeochem. Cycles*, *10*(1), 23–41.

Matsumoto, K., and N. Gruber (2005), How accurate is the estimation of anthropogenic carbon in the ocean? An evaluation of the ΔC^* method, *Global Biogeochem. Cycles*, *19*, GB3014, doi:10.1029/2004GB002397.

Matsumoto, K., et al. (2004), Evaluation of ocean carbon cycle models with data-based metrics, *Geophys. Res. Lett.*, *31*, L07303, doi:10.1029/2003GL018970.

Maybeck, P. S. (1979), *Stochastic Models, Estimation, And Control*, vol. 1, Elsevier, New York.

McNeil, B. I., R. J. Matear, R. M. Key, J. L. Bullister, and J. L. Sarmiento (2003), Anthropogenic CO_2 uptake by the ocean based on the global chlorofluorocarbon data set, *Science*, *299*, 235–239.

Mikaloff Fletcher, S. E., et al. (2006), Inverse estimates of anthropogenic CO_2 uptake, transport, and storage by the ocean, *Global Biogeochem. Cycles*, *20*, GB2002, doi:10.1029/2005GB002530.

Mikaloff Fletcher, S. E., et al. (2007), Inverse estimates of the oceanic sources and sinks of CO_2 in pre-industrial times and their implied oceanic transport, *Global Biogeochem. Cycles*, *21*, GB1010, doi:10.1029/2006GB002751.

NASA (2004), ISLSCP Initiative II [DVD/CD-ROM], U.S. Gov. Print. Off., Washington, D. C.

Orr, J., R. Najjar, C. L. Sabine, and F. Joos (1999), Abiotic-HOWTO, internal OCMIP report, Lab. des Sci. du Clim. et l'Environ., Saclay, France.

Orr, J. C., et al. (2001), Estimates of anthropogenic carbon uptake from four three-dimensional global ocean models, *Global Biogeochem. Cycles*, *15*(1), 43–60.

Pacanowski, R. C., and A. Gnanadesikan (1998), Transient response in a z-level ocean model that resolves topography with partial cells, *Mon. Weather Rev.*, *126*, 3248–3270.

Plattner, G. K., F. Joos, and T. F. Stocker (2002), Revision of the global carbon budget due to changing air-sea oxygen fluxes, *Global Biogeochem. Cycles*, *16*(4), 1096, doi:10.1029/2001GB001746.

Prentice, I., et al. (2001), The carbon cycle and atmospheric carbon dioxide, in *Climate Change 2001: The Scientific Basis*, edited by J. T. Houghton et al., pp. 183–237, Cambridge Univ. Press, New York.

Ramirez, A. J., and A. W. Rose (1992), Analytical geochemistry of organic phosphorus and its correlation with organic-carbon in marine and fluvial sediments and soils, *Am. J. Sci.*, *292*(6), 421–454.

Richey, J. E. (2004), Pathways of atmospheric CO_2 through fluvial systems, in *The Global Carbon Cycle: Integrating Humans, Climate, and the Natural World*, edited by C. B. Field and M. R. Raupach, pp. 329–340, Island, Washington, D. C.

Richey, J. E., J. M. Melack, A. K. Aufdenkampe, V. M. Ballester, and L. L. Hess (2002), Outgassing from Amazonian rivers and wetlands as a large tropical source of atmospheric CO_2, *Nature*, *416*, 617–620.

Rödenbeck, C., S. Houweling, M. Gloor, and M. Heimann (2003a), Time-dependent atmospheric CO_2 inversions based on interannually varying tracer transport, *Tellus, Ser. B*, *55*, 488–497.

Rödenbeck, C., S. Houweling, M. Gloor, and M. Heimann (2003b), CO_2 flux history 1982–2001 inferred from atmospheric data using a global inversion of atmospheric transport, *Atmos. Chem. Phys.*, *3*, 1919–1964.

Sabine, C. L., R. M. Key, K. M. Johnson, F. J. Millero, A. Poisson, J. L. Sarmiento, D. W. R. Wallace, and C. D. Winn (1999), Anthropogenic CO_2 inventory of the Indian Ocean, *Global Biogeochem. Cycles*, *13*(1), 179–198.

Sabine, C. L., et al. (2002), Distribution of anthropogenic CO_2 in the Pacific Ocean, *Global Biogeochem. Cycles*, *16*(4), 1083, doi:10.1029/2001GB001639.

Sarmiento, J. L., and E. T. Sundquist (1992), Revised budget for the oceanic uptake of anthropogenic carbon dioxide, *Nature*, *356*, 589–593.

Sarmiento, J. L., J. C. Orr, and U. Siegenthaler (1992), A perturbation simulation of CO_2 uptake in an ocean general circulation model, *J. Geophys. Res.*, *97*(C3), 3621–3645.

Sarmiento, J. L., C. L. Quéré, and S. W. Pacala (1995), Limiting future atmospheric carbon dioxide, *Global Biogeochem. Cycles*, *9*(1), 121–137.

Siegenthaler, U. (1983), Uptake of Excess CO_2 by an Outcrop-Diffusion Model of the Ocean, *J. Geophys. Res.*, *88*(NC6), 3599–3608.

Takahashi, T., R. A. Feely, R. F. Weiss, D. W. Chipman, N. Bates, J. Olaffson, C. Sabine, and S. C. Sutherland (1999), Net sea-air CO_2 flux over the global oceans: An improved estimate based on the sea-air pCO_2 difference, in *2nd International Symposium, CO_2 in the Oceans*, edited by Y. Nojiri, pp. 9–14, Cent. for Global Environ. Res., Natl. Inst. for Environ. Stud., Tsukuba, Japan.

Takahashi, T., et al. (2002), Global air-sea CO_2 flux based on climatological surface ocean pCO_2, and seasonal biological and temperature effects, *Deep Sea Res., Part II*, *49*, 1601–1622.

Tans, P. P., T. J. Conway, and T. Nakazawa (1989), Latitudinal distribution of the sources and sinks of atmospheric carbon dioxide derived from surface observations and an atmospheric transport model, *J. Geophys. Res.*, *94*(D4), 5151–5172.

Tans, P. P., I. Y. Fung, and T. Takahashi (1990), Observational constraints on the global atmospheric CO_2 budget, *Science*, *247*, 1431–1438.

Wanninkhof, R. (1992), Relationship between wind speed and gas exchange over the ocean, *J. Geophys. Res.*, *97*(C5), 7373–7382.

Wanninkhof, R., and W. R. McGillis (1999), A cubic relationship between air-sea CO_2 exchange and wind speed, *Geophys. Res. Lett.*, *26*(13), 1889–1892.

M. Gloor, A. R. Jacobson, and J. L. Sarmiento, Atmospheric and Oceanic Sciences Program, Princeton University, P.O. Box CN710, Princeton, NJ 08544-0710, USA. (andy.jacobson@noaa.gov)

N. Gruber and S. E. Mikaloff Fletcher, Department of Atmospheric and Oceanic Sciences, University of California, Los Angeles, Los Angeles, CA 90032, USA.